Available online at www.rajournals.in

RA JOURNAL OF APPLIED RESEARCH
ISSN: 2394-6709
DOI:10.47191/rajar/v7i9.03
Volume: 07 Issue: 09 September-2021

International Open Access

Impact Factor- 7.036

Page no.- 2497-2502

Thermal Energy Production and Heat Exchange between an Electrochemical Cell and Its Surroundings

Sarwan S. Sandhu[1], Shane T. Kosir[2], Joseph P. Fellner[3]
[1,2]Department of Chemical and Materials Engineering, University of Dayton, Dayton, OH 45469
[3]Air Force Research Laboratory, Wright-Patterson AFB, OH 45433

ARTICLE INFO

Published Online:
08 September 2021

Corresponding Author:
Sarwan S. Sandhu

ABSTRACT

The theoretical formulation presented in this paper was developed to predict the cell average temperature as a function of time for a given cell discharge current and its initial temperature under adiabatic and nonadiabatic conditions. The cell average temperature versus time data calculated from the derived formulation is presented in the form of plots for an ideal lithium-based button cell (for example, lithium(s)/electrolyte/carbon monofluoride(s)) during its discharge period. The presented data are briefly discussed in light of cell component stability and safe discharge operation.

KEYWORDS: Lithium-ion electrochemical cell, thermal energy production, heat exchange, thermally-safe cell discharge operation

I. INTRODUCTION

On recognition of the need for the development of cleaner and more efficient electrical energy production and storage systems, fundamentals of "Electrochemical Engineering Science" have been applied to acquire the in-depth understanding and accurate formulation of the various transport and electrochemical reaction processes involved in the electrochemical systems such as the polymer electrolyte and battery systems [1-15]. Some examples of the systems utilizing primary/secondary batteries are: national defense systems, ships and airplanes, trucks and cars, laptops, calculators, cell phones, smoke detectors, subway backup power, hearing aids, cameras, clocks, etc. Also, secondary batteries are used to store excess electrical energy generated by systems harnessing renewable energy sources (wind, sun, ocean waves, geothermal), for example, wind turbines, photovoltaic cells, and water turbines, as well as that generated by fossil fuel combustion-based power plants. Generally, the electrochemical performance behavior of a given lithium-based cell during its discharge or charge depends on its temperature at a constant discharge or charge current. During the transient cell discharge period, a fraction of the Gibbs free energy change of the overall cell reaction is converted into thermal energy. Depending on the thermal design of a cell for its operation at a desired current level, a fraction of the produced thermal energy would accumulate in the cell interior; consequently, causing a rise in the cell temperature. The cell average temperature would continue to rise and may exceed the safe operating temperature limit of a poor cell thermal design. Therefore, it is of paramount importance to investigate the cell temperature as a function of time at each current level intended to be used during the discharge period of a lithium-based cell as well as determine the safe operating temperature range during its discharge period. To this end, we present the thermal model below.

During the discharge period of a lithium-based cell, for example: $Li(s)/electrolyte/CF_x\ (s), x = 1$; thermal energy is generated due to the occurrence of irreversible ionic and electronic transport in the cell electrolyte and electrodes, and electrochemical reaction kinetics charge-transfer polarization processes at the cell electrode-electrolyte interfaces. Depending on the cell discharge current, the rate of change of the entire cell-mass averaged temperature with time would depend on the thermal energy production and the loss of the cell thermal energy content in the form of heat transfer to the environment surrounding the cell. The mathematical formulation presented in Section II is an attempt to predict the transient average cell temperature for a lithium-based cell, such as the 'model' button cell shown in Figure 1. During the cell discharge period at a cell current level, lithium ions are transferred from the lithium sheet anode into the electrolyte solution held in the cell porous separator whereas electrons are transferred to an external circuit. Lithium ions migrate through the electrolytic solution to the active sites of the composite cathode active material (such as $CF_x\ (s), x = 1$) particles for the reaction with the active material in the presence of electrons provided by the cathode current collector via an electronic conductor such as carbon black; noting that the current collector receives electrons from the cell external circuit.

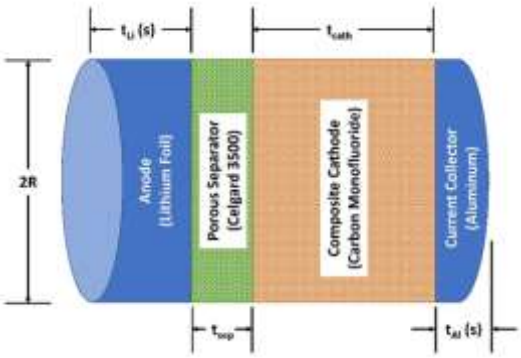

Figure 1. Sketch of the 'model' button cell: $Li(s)/electrolyte/CF_x\ (s), x = 1$ (not to scale). The button cell, as shown here, is uncased (bare) with no leads.

Dimensions, masses, and physical property information about the major components of the button cell shown in Figure 1 are provided in the Supplementary Material.

II. FORMULATION

The developed formulation presented in this section has been exclusively employed to predict the temperature versus time behavior of the 'model' button cell depicted in Figure 1. The formulation, however, with some adjustment, can be applied for the prediction of the transient average temperature for any type of galvanic cell during its discharge as a function of time or its capacity exhausted to store charge in its cathode active material.

During the cell discharge period at a constant current, I amperes, the thermal energy production rate [16] is given by:

$$\dot{P}_{thermal} = I\left[E - E_{OCV} + T\left(\frac{\partial E_{OCV}}{\partial T}\right)_{P,DOD}\right] \qquad (1)$$

where E is the actual cell electric potential [volt], E_{OCV} is the open-circuit cell potential [volt], $\left(\frac{\partial E_{OCV}}{\partial T}\right)_{P,DOD}$ is the change of E_{OCV} per unit change in cell temperature at the constant pressure and depth of cell discharge (DOD). If the information on $\left(\frac{\partial E_{OCV}}{\partial T}\right)_{P,DOD}$ is either not available or its value is so small that the numerical value of $\left[T\left(\frac{\partial E_{OCV}}{\partial T}\right)_{P,DOD}\right]$ is insignificant relative to $(E - E_{OCV})$ for a given electrochemical cell; then, it is appropriate to assume that

$$\dot{P}_{thermal} = (E - E_{OCV}) \qquad (2)$$

II.A. Galvanic Cell Discharge under Adiabatic Conditions (I.E., Zero Heat Exchange between the Galvanic Cell Body 'Skin' Surface and Its Surrounding Environment)

The general transient thermal energy balance over a galvanic cell; for example, the 'model' button cell depicted in Figure 1; is:

$$\begin{pmatrix}rate\ of\ thermal\ energy\ accumulation\ in\ the\ cell\\ material\ components\end{pmatrix} =$$

$$\left[\begin{pmatrix}\text{rate of thermal energy production assiciated with the cell voltage}\\ \text{loss because of irreversible occurrence of transport of ions and electrons}\\ \text{in the various components of the cell as well as the electrochemical}\\ \text{reactions at the cell eletrolyte-electrode active material component interfaces}\end{pmatrix} + \begin{pmatrix}\text{rate of reversible thermal energy prodution}\end{pmatrix}\right] +$$

$$-\begin{pmatrix}rate\ of\ loss\ of\ thermal\ energy\ from\ the\ cell\ body\ skin\ sur\\ in\ the\ form\ of\ heat,\ to\ the\ cell\ surrounding\ environmer\end{pmatrix} \qquad (3)$$

For cell operation under adiabatic conditions, the heat loss term in Eq. (3) is, by definition, zero. Therefore, Eq. (3) becomes:

$$\begin{pmatrix}rate\ of\ thermal\ energy\ accumulation\\ in\ all\ the\ cell\ material\ components\end{pmatrix} = (rate\ of\ thermal\ energy\ production) \qquad (4)$$

Expressing Eq. (4) in mathematical symbols and simplifying leads to $\frac{dT}{dt} = \frac{|\dot{P}_{thermal}|}{\sum_j m_j C_{p,j}} = \left[\frac{|I(E-E_{OCV})|}{\sum_j (m_j C_{p,j})}\right]$ (5)

where m_j is the mass of a cell material component, j, [g], $C_{p,j}$ its heat capacity, $[Jg^{-1}K^{-1}]$, T the cell average temperature [K] at the discharge time, t [sec], during the cell discharge period. Equation (5) is solved using the initial condition: at $t = 0\ sec, T = T_{ini}\ [K]$.

$$\int_{T_{ini}}^{T} dT = \int_0^t \left[\frac{|I(E-E_{OCV})|}{\sum_j (m_j C_{p,j})}\right] dt \qquad (6)$$

$$(T - T_{ini}) = \int_0^t \left[\frac{|I(E-E_{OCV})|}{\sum_j (m_j C_{p,j})}\right] dt \qquad (7)$$

Expressing Eq. (7) in dimensionless form by defining θ_{temp} as:

$$\theta_{temp} = \frac{T - T_{ini}}{T_{ini}} = \int_0^t \left[\frac{|I(E-E_{OCV})|}{T_{ini}\sum_j (m_j C_{p,j})}\right] dt \qquad (8)$$

For the situation of a galvanic cell operating under the adiabatic conditions when the overall function within square brackets, […], changes with time, the right-hand side of Eq. (8) can be integrated numerically using an integration technique, such as Simpson's rule [17]. For the acceptable assumption of constant $\sum_j (m_j C_{p,j})$ as well as negligible variation [18] in $(E - E_{OCV})$ with time at a constant current I during the cell discharge period, Eq. (8) becomes

$$\theta_{temp} = \frac{T - T_{ini}}{T_{ini}} = \frac{I|E-E_{OCV}|t}{(T_{ini}\sum_j m_j C_{p,j})} \qquad (9)$$

II.B Galvanic Cell Discharge Under Nonadiabatic Conditions. Heat Exchange between the Cell 'Skin' Surface and Its Surrounding Environment via Natural Convection And Radiative Heat Transfer

The thermal energy balance applied over the galvanic cell system at any time during its discharge period is the same as Eq. (3).

$$\text{Rate of thermal energy production} = \mathbf{I\left|\left(E - E_{OCV}\right)\right|} \qquad (10)$$

Rate of thermal energy accumulation $= \left(\sum_j \mathbf{m_j C_{p,j}}\right)\frac{\mathbf{dT}}{\mathbf{dt}}$ (11)

Rate of thermal energy loss as heat from the cell surface to its surroundings (via the combined effect of natural and radiative heat transfer processes [19,20])

$= \left[\sum_j \left(\mathbf{h_c + h_{r,j}}\right)\left(\mathbf{T - T_{surr}}\right)\mathbf{A_{surf,j}}\right]$ (12)

Inserting the information in Eq. (10) through (12) into Eq. (3) and simplifying leads to

$$\frac{dT}{dt} = \frac{\{I|(E-E_{OCV})|-\sum_j[(h_c+h_{r,j})(T-T_{surr})A_{surf,j}]\}}{(\sum_j m_j C_{p,j})} \quad (13)$$

where h_c is the natural convection heat transfer coefficient for heat transfer through the thermal boundary layer around the outer 'skin' surface of a cell component j $[Js^{-1}cm^{-2}K^{-1} = Wcm^{-2}K^{-1}]$, $h_{r,j}$ is the radiative heat transfer coefficient for heat transfer from the outer 'skin' surface from the cell component j $[Js^{-1}cm^{-2}K^{-1} = Wcm^{-2}K^{-1}]$, $A_{surf,j}$ is the area of the outer skin surface of the cell component j $[cm^2]$, T_{surr} the temperature of the environment around the cell [K], and T the cell average temperature [K] at any time, t (sec), during the cell discharge period. One should note that

$$\mathbf{h_{r,j}\left(T - T_{surr}\right) = \sigma\, \varepsilon_{s,j}\left(T^4 - T_{surr}^4\right)} \quad (14)$$

where

$\sigma =$ the Stefan-Boltzmann constant and $\varepsilon_{s,j} =$ emissivity of the surface of compnent j.

Section II.C provides more pertinent information on the natural convection and radiative heat transfer coefficients.

In general, Eq. (13) can be solved for the cell temperature T as a function of time, t, for a constant or varying cell current using a numerical method such as the Euler method or Runge-Kutta method [21,22]. For the analytical solution, Eq. (13) is as expressed as:

$$\frac{d(T-T_{surr})}{dt} = \frac{\{I|(E-E_{OCV})|-(\sum_j[(h_c+h_{r,j})A_{surf,j}])(T-T_{surr})\}}{(\sum_j m_j C_{p,j})} \quad (15)$$

The heat loss rate from the cell at its initial temperature, $T = T_{ini}$;

$$\dot{q}_{tot,ini} = \left(\sum_j\left[\left(h_c + h_{r,j}\right)A_{surf,j}\right]\right)\left(T_{ini} - T_{surr}\right) \quad (16)$$

If the thermal energy production rate$= \dot{P}_{thermal} = [I|(E - E_{open})|]$ is greater than $\dot{q}_{tot,ini}$; the cell temperature would start rising with an increase in the cell discharge time. The cell temperature would continue to increase until either the cathode active material capacity to hold charge or lithium amount is completely exhausted or if the cell temperature approaches the melting point of the lithium metal or any other cell component.

For the assumption of $\dot{P}_{thermal} = [I|(E - E_{open})|]$ being approximately constant, as is observed in the case of discharge of a cell; e.g., $[Li(s)/electrolyte/CF\ (s),$ cell] at a constant current, with $(E - E_{open})$ remaining approximately invariant over its significant discharge period [18,23] and with the additional assumption of insignificant or slight variation in $(\sum_j[(h_c + h_{r,j})A_{surf,j}])$, the following analytical solution of Eq. (15) was obtained:

$$\int_{(T-T_{surr})=(T_{ini}-T_{surr})}^{(T-T_{surr})=(T-T_{surr})} \frac{d(T-T_{surr})}{I|(E-E_{OCV})|-(\sum_j[(h_c+h_{r,j})A_{surf,j}])(T-T_{surr})} = \int_{t=0}^{t=t}\left(\frac{dt}{(\sum_j m_j C_{p,j})}\right) = \frac{t}{(\sum_j m_j C_{p,j})} \quad (17)$$

The left-hand side integral was obtained using the information provided in [25] and the resultant equation obtained from Eq. (17) was further simplified to obtain:

$$(T - T_{surr}) = \frac{1-[1-\zeta(T_{ini}-T_{surr})]e^{-\xi t}}{\zeta} \quad (18)$$

Or, $\theta_{temp-nonadiabatic} = \left(\frac{T-T_{surr}}{T_{surr}}\right) = \frac{1-[1-\zeta(T_{ini}-T_{surr})]e^{-\xi t}}{\zeta T_{surr}}$ (19)

for $\dot{P}_{thermal}(= |I(E - E_{open})|) > \dot{q}_{tot,ini}\left[= (\sum_j[(h_c + h_{r,j})A_{surf,j}])\left(T_{ini} - T_{surr}\right)\right]$ (20)

where $\zeta = \frac{\sum_j(h_c+h_{r,j})A_{surf,j}}{I|(E-E_{open})|}, [K^{-1}]$ (21)

$$\xi = \frac{\sum_j(h_c+h_{r,j})A_{surf,j}}{\sum_j(m_j C_{p,j})}, [s^{-1}] \quad (22)$$

All the algebraic steps to arrive at the final expression in Eq. (19) are not shown here for the sake of brevity.

For the case where $\dot{P}_{thermal}\ (= |I(E - E_{open})|) < \dot{q}_{tot,ini}\left[= (\sum_j[(h_c + h_{r,j})A_{surf,j}])\left(T_{ini} - T_{surr}\right)\right]$the cell body cooling starts from the very beginning of the galvanic cell discharge. For this case, the appropriate differential form of the thermal energy balance over the cell during its discharge period at any time is given as

$$\left(-\frac{dT}{dt}\right) = \frac{\{\sum_j[(h_c+h_{r,j})(T-T_{surr})A_{surf,j}]\}-(I|E-E_{OCV}|)}{(\sum_j m_j C_{p,j})} \quad (23)$$

Or, $$\left[-\frac{d(T-T_{surr})}{dt}\right] = \frac{\{\sum_j[(h_c+h_{r,j})(T-T_{surr})A_{surf,j}]\}-(I|E-E_{OCV}|)}{(\sum_j m_j C_{p,j})} \quad (24)$$

Solution of this differential equation leads to:

$$\theta_{temp-nonadiabatic} = \left(\frac{T-T_{surr}}{T_{surr}}\right) = \frac{1+[\zeta(T_{ini}-T_{surr})-1]e^{-\xi t}}{\zeta T_{surr}} \quad (25)$$

for the case where $\dot{P}_{thermal}(= |I(E - E_{open})|) < \dot{q}_{tot,ini}\left[= (\sum_j[(h_c + h_{r,j})A_{surf,j}])\left(T_{ini} - T_{surr}\right)\right]$ (26)

where T_{ini} =initial temperature of the cell [K].

The cell cooling, as suggested by Eq. (25), would continue until the cathode active material capacity to store lithium or charge would be completely exhausted.

II.C Natural Convection and Radiation Heat Transfer Coefficients

For the situation of temperature, T, of a cell component j being equal to the temperature of the environment surrounding the cell, T_{surr}, the heat transfer coefficient, h_c, can be computed from the following equation [19]:

$$Nu_f = \frac{h_c D}{k_f} = 0.45 \tag{27}$$

where Nu_f is the Nusselt number for heat transfer; h_c is the natural convection-conduction heat transfer coefficient for the transfer of heat through the thermal boundary layer around a cell of the cylindrical type of diameter, D, $[Js^{-1}cm^{-2}K^{-1}]$; D is the diameter of the cylindrical-type cell, [cm]; k_f is the thermal conductivity of the surrounding air, $[Js^{-1}cm^{-1}K^{-1}]$, at the film temperature, $T_f = \frac{T+T_{surr}}{2}, [K]$.

For $\Delta T = (T - T_{surr}) > (a\ few\ degrees)$, h_c can be estimated from

$$Nu_f = \frac{h_c D}{k_f} = 0.53\left(Gr_f Pr_f\right)^{0.25} \tag{28}$$

Eq. (28) is valid for $Gr_f Pr_f = 10^3 - 10^9$. The Grashof number for heat transfer, by definition, is: $Gr_f = \left[D^3 g\beta_f(\Delta T)\left(\frac{\rho_f}{\mu_f}\right)^2\right] = \left[\frac{D^3 g\beta_f(\Delta T)}{\nu_f^2}\right]$; the Prandtl number for heat transfer, $Pr_f = \frac{C_{p,f}\mu_f}{k_f}$; acceleration due to the gravitational effect, $g = 981.0, [cms^{-2}]$; coefficient of thermal expansion of air following ideal-gas behavior at the film temperature, $\beta_f = \frac{1}{T_f}, [K^{-1}]$; cell surrounding air density, $\rho_f, [gcm^{-3}]$, dynamic viscosity, $\mu_f, [gcm^{-1}s^{-1}]$, and kinematic viscosity, $\nu_f, [cm^2s^{-1}]$, at the film temperature and atmospheric pressure; the cell surrounding air thermal conductivity, $k_f, [Js^{-1}cm^{-1}K^{-1}]$, and heat capacity at constant pressure, $C_{p,f}, [Jg^{-1}K^{-1}]$. For the values of $(GrPr)_f = Gr_f Pr_f$ outside the range of $10^3 - 10^9$, see Fig. 7-11 [19] or Fig. 12-8 [20].

The radiative heat transfer coefficient, $h_{r,j}$, for heat exchange between the 'skin' surface of component j of the galvanic cell of surface area, $A_{surf,j}$, and emissivity, $\varepsilon_{s,j}$, is given by:

$$h_{r,j} = \frac{\sigma\varepsilon_{s,j}\left(T^4 - T_{surr}^4\right)}{T - T_{surr}} \tag{29}$$

For the situation of $\Delta T = (T - T_{surr}) = 0$, or $\Delta T < 5\ K$, Eq. (28) is reduced [20] to:

$$h_{r,j} \approx 4\sigma\varepsilon_{s,j}T^3 \tag{30}$$

where $\sigma = 5.67051 \times 10^{-8}\ [Wm^{-2}K^{-4}] = 5.67051 \times 10^{-12}\ [Wcm^{-2}K^{-4}]$is the Stefan-Boltzmann constant [24]. If ΔT is more than a few degrees but less than 20% of the absolute surface temperature, $T, [K]$, then $T_f = \left(\frac{T+T_{surr}}{2}\right)$ is recommended [20] for use in Eq. (30) in place of T to improve the accuracy.

III. COMPUTATIONS USING THE MODEL EQUATIONS

The parametric information about the 'model' button cell depicted in Figure 1 was employed to calculate the dimensionless temperature, $\theta_{temp} = \frac{T-T_{ini}}{T_{ini}}$, versus time from Eq. (9) under adiabatic discharge conditions for typical cell currents of 0.0182, 9.1×10^{-4}, 4.55×10^{-4}, and 1.138×10^{-4} A, and the corresponding $\left|E - E_{theoretical,OCV}\right| = |E - 4.57|$ voltages [18,23]. For the nonadiabatic cell discharge operation, $\theta_{temp} = \frac{T-T_{surr}}{T_{surr}}$ versus time was computed from Eq. (19) for the case of $\dot{P}_{thermal} > \dot{q}_{tot,ini}$; and from Eq. (25) for the case of $\dot{P}_{thermal} < \dot{q}_{tot,ini}$ for the above-mentioned cell discharge currents.

IV. RESULTS AND DISCUSSION

Figure 2 shows the cell temperature versus time plots for the 'model' button cell discharge under the adiabatic conditions for the cell currents. The dimensionless temperature, $\theta_{temp} = \frac{T-T_{ini}}{T_{ini}}$, varies linearly with the cell discharge time. The average cell temperature rise rate at the cell '1C' discharge rate is very high relative to the other cell discharge currents. It should be noted that corresponding to any cell discharge time, the cell cathode active material capacity exhausted to hold charge (or lithium amount) at a constant cell discharge current is given by: (It). The theoretical capacity for the 'model' button cell depicted in Figure 1 is, $Q_{theoretical} = 0.0182\ Ah$. So, at a given cell discharge current, I, one can always determine the maximum discharge time. However, if the average cell temperature approaches very close to the melting point of lithium metal, acting as the cell anode, in a time period shorter than the maximum discharge time required to utilize the cathode active material capacity depending on the cell discharge current; the cell discharge must be stopped to avoid damage to the cell components and its rupture (for the case of cell inadequate design pressure) due to the internal pressure rise because of the vaporization of the solvent of the cell electrolytic solution. For example, the vapor pressure of the solvent dimethoxy-ethane (DME) used as an electrolytic solution at 180.5°C (the melting point of Li (s)) is 10.25 bar. One should also realize that other cell components such as the Celgard separator and PVDF binder would melt before the melting of the cell anode, lithium metal sheet. This situation would lead to the failure of the galvanic cell to deliver electric power to an external circuit.

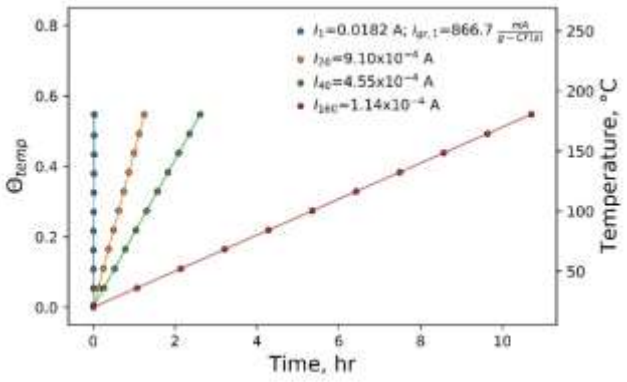

Figure 2. Plot of $\theta_{temp} = \frac{T-T_{ini}}{T_{ini}}$ versus time, t [hr]. Cell discharge at the current levels shown is under adiabatic conditions; $T_{ini} = 293.15\ K$.

Figure 3 shows the dimensionless cell temperature, $\theta_{temp} = \frac{T-T_{surr}}{T_{surr}}$, as well as the actual cell average temperature, T, versus time for the four cell currents under the nonadiabatic conditions where the heat exchange between the cell outer 'skin' surface and its surrounding environment can take place via the natural convection and radiation mechanisms. For the discharge currents of 0.0182 and $9.1 \times 10^{-4}\ A$, heating of the cell takes place. Eventually, the cell average temperature reaches its steady-state value in each case in a time period shorter than the time required for the complete utilization of the cathode active material capacity to store charge. Also, it is apparent that the steady-state temperatures are safe for its discharge operation for these cell currents. One should realize that, at the steady-state cell temperature, the thermal energy production rate in the cell is equal to the rate of heat loss from the cell to its surrounding environment. For the cell currents of 4.55×10^{-4}, and $1.14 \times 10^{-4}\ A$, cell cooling is represented. For each of these currents, the cell average temperature decreases and reaches its steady-state value as shown in Figure 3. Figure 4 is the amplification of the $\theta_{temp} = \frac{T-T_{surr}}{T_{surr}}$ versus time plot for $I_{40} = 4.55 \times 10^{-4}\ A$, $T_{ini} = 323.15$ K (= 50°C) and $T_{surr} = 293.15$ K (= 20°C).

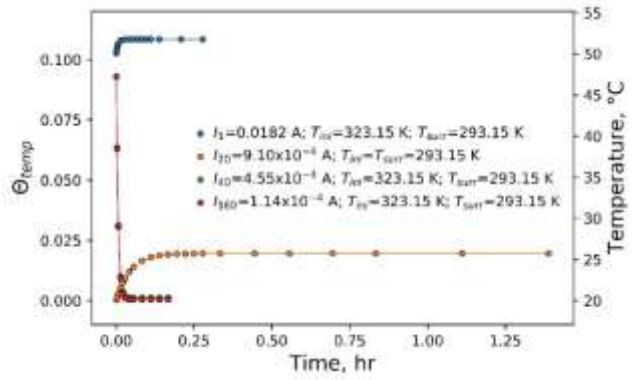

Figure 3. Plot of $\theta_{temp} = \frac{T-T_{surr}}{T_{surr}}$ versus time for the nonadiabatic discharge operation of the galvanic 'model' button cell.

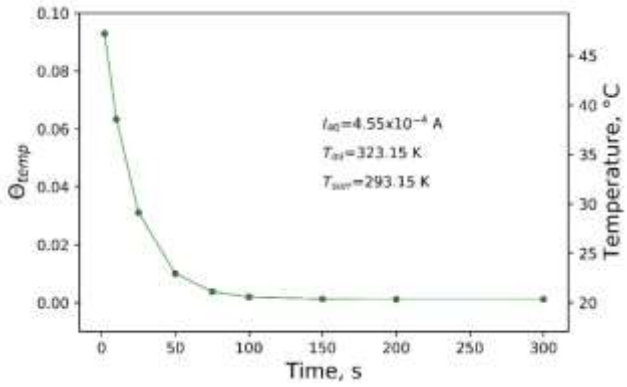

Figure 4. Plot of $\theta_{temp} = \frac{T-T_{surr}}{T_{surr}}$ versus time for the nonadiabatic discharge operation of the galvanic 'model' button cell (amplification).

V. CONCLUSION

The formulation presented in this paper was developed to predict the average cell temperature of a lithium-based electrochemical cell for its discharge at a given cell current and initial temperature under adiabatic and nonadiabatic conditions. The predicted average cell temperature versus time profiles show the linear behavior for the discharge of the lithium-based 'model' button cell, Li(s)/electrolyte/CF(s), discharged at a fixed current level under adiabatic operational conditions. The cell average temperature could reach the melting point (180.5°C) of the solid lithium sheet (acting as the cell anode) before the cell composite cathode active material capacity to hold charge is completely exhausted. Note that at this temperature, the predicted vapor pressure of the solvent, dimethoxy-ethane (DME) is 10.25 bar. For the nonadiabatic operation of the cell, where the heat exchange between the cell outer surface and its surrounding environment takes place via both the natural convection and radiative heat transfer mechanisms, cell heating ensues for the discharge currents of 0.0182 A and $9.1 \times 10^{-4}\ A$ whereas for the cell discharge currents of 4.55×10^{-4} and $1.14 \times 10^{-4}\ A$, cell cooling starts from the beginning of the cell discharge. The cell dimensionless temperature, $\theta_{temp} = \frac{T-T_{surr}}{T_{surr}}$, reaches its steady-state value in each case long before the complete exhaustion of the composite cathode active material capacity to hold charge.

Finally, it is stated here that the developed analytical formulation presented in this paper, with some adjustment, can be employed to predict the average cell temperature as a function of time for any galvanic cell during its discharge at a fixed cell current level for operation under adiabatic and nonadiabatic conditions. The predicted cell average temperature versus time information is of paramount importance for the safe operation of a galvanic cell at any cell current level. It is strongly recommended to determine the cell temperature versus time data through a carefully designed experimental program to validate the models presented in Sections II.A and II.B.

REFERENCES

1. Fellner JP, Sandhu SS. Diffusion-limited self-discharge reaction in the Hubble space telescope battery. Journal of PowerSource. 1996;58:99-102. doi:10.1016/0378-7753(96)02329-4
2. Fellner JP, Sandhu SS. Diffusion-limited model for a lithium/polymer battery. Electrochim Acta. 1998;43(10-11):1607–1613. doi:10.1016/S0013-4686(97)10061-5
3. Sandhu SS, Crowther RO, Krishnan SC, Fellner J. Direct Methanol Polymer Electrolyte Fuel Cell Modeling: Reversible Open-Circuit Voltage and Species Flux Equations. Electrochem Acta. 2003;48:2295-2303.
4. Sandhu SS. High Temperature PBO Based Solid Polymer Electrolyte Fuel Cell Development.; 2002.Technical Report
5. Sandhu SS, Crowther RO, Fellner JP. Prediction of methanol and water fluxes through a direct methanol fuel cell polymer electrolyte membrane. Electrochim Acta. 2005;50(19):3985-3991. doi:10.1016/j.electacta.2005.02.048
6. Sandhu SS, Fellner JP. Model formulation and simulation of a solid-state lithium-based cell. Electrochim Acta. 2013;88:495-506. doi:10.1016/j.electacta.2012.10.110
7. Sandhu SS, Fellner JP. Characterization of Iron Phthalocyanine as the Cathode Active Material for Lithium-Ion Batteries. J Chem Eng Process Technol. 2015;06(05). doi:10.4172/2157-7048.1000257
8. Sandhu SS, Fellner JP, Tsao M, Cashion CJ. Electrochemical characterization of the high charge capacity copper phthalocyanine for primary batteries. Int J Eng Technol Manag Appl Sci. 2017; 5(11).
9. Fellner JP, Scanlon LG, Tsao M, Tsao B, Sandhu SS, Lawson J. High Capacity Materials Functionalized with Carbon for Lithium-Ion Batteries.; 2017.
10. Sandhu SS, Fellner JP. Ab-initio calculations for lithium/diquinoxalinylene battery. Invent J Res Technol Eng Manag. 2020;4(1):6-10.
11. Sandhu SS, Cashion CJ, Fellner JP. Mathematical Model for Lithium-Ion Intercalation into the Cathode Active Material of a Lithium-Based Cell/Battery. RA J.2019;05(02):2324-2328. doi:10.31142/rajar/v5i2.07
12. Sandhu SS, Cashion CJ, Fellner JP. Theoretical and Experimental Characterizations of a Rechargeable Hybrid Cathode for Lithium-Based Batteries. In: AIChE Annual Meeting. Pittsburgh; 2018.
13. Sandhu SS, Fellner JP. Development of high performance organic-based cathodes. In: AIChE Spring National Meeting. ; 2020.
14. Sandhu .S., Kosir S. Overall Semi-Empirical Rate-Law Formulation of a Lithium-Based Cell or Battery. RA J Appl Res. 2020;06(08):2708-2712. doi:10.47191/rajar/v6i8.01
15. Sandhu SS, Kosir S. Rate-Law Application To Simulate Lithium-Based Cell Experimental Data. RA J Appl Res. 2020;06(12):2807-2809. doi:10.47191/rajar/v6i12.06
16. Newman J, Thomas-Alyea KE. Electrochemical Systems. Wiley; 2004.
17. Felder RM. Elementary Principles of Chemical Processes. Wiley; 1978.
18. Zhang S., Foster D., Wolfenstine J., Read J. Electrochemical Characteristics and Discharge Mechanism of a Primary Li/CFx Cell. Journal of Power Sources 187 (2009) 233-237.
19. McAdams WH. Heat Transmission. McGraw-Hill; 1954.
20. McCabe WL, Smith JC, Harriot P. Unit Operations of Chemical Engineering. pp.376-379, 434, 435 (7th ed. McGraw-Hill; 2005).
21. Spiegel MR. Advanced Mathematics for Engineers and Scientists. McGraw-Hill; 1971.
22. Carnahan B, Luther HA, Wilkes JO. Applied Numerical Methods. Wiley; 1969.
23. Read J, Foster D, Wolfenstine J, Zhang S. Microcalorimetry of Li/CFx Cells and Discharge Mechanism.; 2009.
24. Bird RB, Stewart WE, Lightfoot EN. Transport Phenomena., p. 867,2nd ed. Wiley; 2007.
25. Spiegel MR. Mathematical Handbook of Formulas and Tables. McGraw-Hill; 1968.